Nanoparticle diffusion on desorbing solids: The role of elementary excitations in buffer-layer-assisted growth

V. N. Antonov,[1] J. S. Palmer,[2] P. S. Waggoner,[2] A. S. Bhatti,[2,*] and J. H. Weaver[1,2]
[1]*Department of Physics, University of Illinois at Urbana-Champaign, Urbana, Illinois 61801, USA*
[2]*Department of Materials Science and Engineering, and Frederick Seitz Materials Research Laboratory, University of Illinois at Urbana-Champaign, Urbana, Illinois 61801, USA*
(Received 27 February 2004; published 9 July 2004)

Physical vapor deposition onto rare gas buffer layers leads to the spontaneous formation of clusters. During the thermal desorption of the buffer, these clusters diffuse and aggregate into larger structures, a process known as buffer-layer-assisted growth and desorption assisted coalescence. We studied the effect of buffer thickness and the rate of buffer desorption on the extent of this aggregation for Ag, Au, Cu, Pd, Co, and Ni particles on a solid Xe surface. On the basis of these experiments, results from Monte Carlo simulations and the existing theoretical models for cluster–cluster aggregation, we report for the first time the Arrhenius parameters for nanoparticle slip-diffusion. The effective activation energies range from 0.12 for small Ag clusters (few hundred atoms) to 0.60 eV for ramified Ni islands (millions of atoms), and the giant pre-exponential factors were found to differ by many orders of magnitude. Significantly, the pre-exponential factors follow a Meyer–Neldel-type dependence on the corresponding effective activation energy, with a characteristic Meyer–Neldel energy of 6.9 meV. This energy is associated with the phononic excitations in solid Xe that are responsible for nanostructure mobility. This dependence should be a characteristic feature of nanoparticle diffusion.

DOI: 10.1103/PhysRevB.70.045406 PACS number(s): 68.65.−k, 68.43.Jk, 68.35.Ja, 65.80.+n

I. INTRODUCTION

Nanostructure self-assembly is currently a topic of considerable interest, and insights into the physics underlying the surface mobility of nanoscale particles are especially germane.[1,2] A particularly interesting case of cluster/nanostructure diffusion on a solid surface is observed during a process known as buffer-layer-assisted growth (BLAG), which was introduced by Huang *et al.*,[3] following earlier work by Waddill *et al.*[4,5] In BLAG, atoms are vapor-deposited onto thin layers of rare gas solids that have been grown at 20–50 K on a substrate of choice.[6] Clusters form spontaneously due to weak bonding with the buffer. Subsequent warm-up activates cluster diffusion, aggregation, and coalescence on the subliming buffer layer. In this way, nanostructures establish contact by soft-landing on a pristine surface.[7–9] Their interactions with the substrate can then be examined and their intrinsic properties can be explored. Of interest in this paper is cluster diffusion and aggregation on the buffer layer, with emphasis on the activation energies and pre-exponents for atomically clean nanostructures that may range from compact clusters of a few hundred atoms to extended ramified islands with 10^8 atoms and a characteristic length of up to a few microns.

BLAG was initially utilized to fabricate atomically abrupt metal-semiconductor junctions in studies of Schottky barrier formation.[5,7] Subsequently, it was discovered that the average size of the nanostructures could be varied over several orders of magnitude by suitable choice of buffer-layer thickness.[3] More recently, it was demonstrated that the fractal (Haussdorff) dimension of ramified islands formed by BLAG is consistent with Monte Carlo simulations of diffusion-limited cluster–cluster aggregation.[10] This suggests that the clusters experience fast Brownian motion.

In a recent study, we focused on the physical origins of BLAG by studying the growth of Au nanostructures on solid Ar, Kr, and Xe.[11] From the normalized size distributions of compact cluster and large fractal islands, we found that the diffusivity scales as the inverse of the island-buffer contact area. This indicates that diffusion is controlled by viscous friction at the highly incommensurate interface. We proposed a simple model for BLAG which qualitatively explained the observed dependence of island density on buffer layer thickness as resulting from competition between the rates of island diffusion and buffer desorption. Our findings also implied that the effective activation energy for diffusion was very weakly, if at all, dependent on the island size. Thus, diffusivity is the product of two terms that depend on the contact area S and on temperature T, $D(S,T)=D_S(S)D_T(T)$, where the temperature-dependent part follows the Arrhenius behavior:

$$D_T(T) = D_{00}\exp(-\varepsilon_d/kT). \tag{1}$$

Here, ε_d is the effective activation energy of the process, k is the Boltzmann constant, and D_{00} is a prefactor independent of size or temperature.

This paper focuses on the kinetic parameters for diffusion of compact clusters of Ag and Au and of large ramified islands of Au, Cu, Pd, Co, and Ni. These were chosen because they are representative of the transition metal and the noble metal groups, and all exhibit close-packed structures. Here, Xe is the buffer-layer material, but analogous results would be expected for other weakly binding incommensurate supports. Previously, quantitative analysis of the experimental data on the basis of our model was hindered by several problems: (1) heat released from coalescence that could affect the diffusion rates,[11] (2) fragmentation of small ramified

particles,[12] and (3) a lack of theoretical models that could describe the high-coverage regime of aggregation (nondilute limit) where the first two problems do not appear. In the compact regime, as exemplified by Ag and Au, problems (1) and (2) were overcome by limiting the analysis to certain ranges of buffer-layer thickness. To analyze aggregation when the surface coverage was far from the dilute limit, problem (3), we carried out Monte Carlo simulations of two-dimensional cluster–cluster aggregation. These simulations made it possible to determine the diffusion parameters for ramified nanostructures of Au, Cu, Co, Pd, and Ni. From this data set, we find relatively large effective activation energies and gigantic diffusion prefactors that follow a Meyer–Neldel-type relationship.[13] The calculated Meyer–Neldel energy is comparable to the Debye energy of solid Xe, showing the many-body nature of particle diffusion.

II. EXPERIMENT

The samples were grown in an ultrahigh-vacuum chamber with a typical base pressure $<1\times10^{-10}$ Torr. The substrates were 20–30 nm thick amorphous carbon (a-C) films supported on copper grids. A closed-cycle He refrigerator was used to cool the samples to 20 K, and the temperature was measured with a AuFe–Chromel thermocouple. Growth of the buffer layer occurred when Xe gas was introduced into the chamber to raise the pressure to 1×10^{-6} Torr. The pressure was monitored with an ion gauge, corrected for Xe sensitivity. The buffer growth rate was estimated from the number of incident atoms per unit time per unit area, namely $I=p/(2\pi mkT)^{1/2}$, where p is the partial Xe pressure, m is the mass of a Xe atom, T is the ambient temperature, and the sticking coefficient was assumed to be unity.[14] Following buffer-layer formation, the metal atoms were evaporated from tungsten (Ag, Cu, and Au) or Al_2O_3-coated tungsten baskets (Co, Ni, and Pd). The impinging adatoms were sufficiently mobile on solid Xe to form clusters, a process favored by weak bonding with the rare gas solid. Though the temperature was ~20 K, atom capture by a cluster would release an amount of heat comparable to the material cohesive energy, facilitating atom rearrangement. Sublimation of the buffer was achieved when the cold head was warmed, and cluster aggregation occurred during this time. With a resistive heater mounted between the samples and the refrigerator head, we could control the warm-up rate β. The new results presented here were for β between 0.05 and 2.75 K min^{-1}. The results of Huang *et al.*[3] for very small Ag nanostructures were obtained from samples that were physically removed from the cold head. In that case, the particle densities were obtained *in situ* with a scanning tunneling microscope (STM) at room temperature.

Characterization of the samples grown here was done after their transfer to a Philips CM12 120 kV transmission electron microscope (TEM). Imaging was done in the bright-field mode, keeping the beam intensity low to avoid significant changes in nanostructure morphology. The number of nanostructures per unit area was determined directly from the TEM micrographs, where each contiguous structure was counted as a single particle. The samples were stable when stored in air, although the oxidation of the Cu nanostructures was clearly visible in the TEM. No evidence for island coarsening was observed.

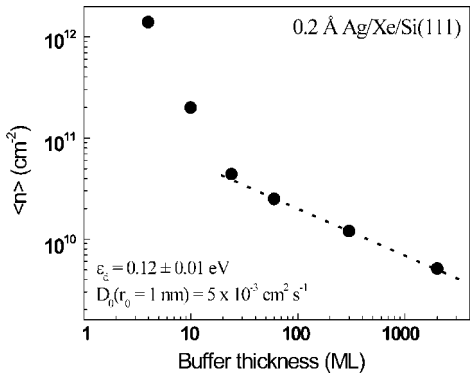

FIG. 1. Ag cluster densities for compact clusters as a function of Xe buffer thickness, resulting from deposition of 0.2 Å Ag and subsequent desorption of Xe (from Ref. 3). The densities follow a power law in the limit of large buffer thickness, consistent with an effective activation energy for diffusion $\varepsilon_d=0.12\pm0.01$ eV and a prefactor of 5×10^{-3} cm^2 s^{-1} for clusters of 1 nm radius. The density behavior on thin buffers is influenced by heat released when clusters coalesce (Ref. 11).

III. RESULTS AND DISCUSSION

A. Compact particle aggregation: Dependence on buffer-layer thickness

Recent studies of BLAG by Huang *et al.*[3] focused on the aggregation of small Ag clusters on a desorbing Xe buffer. Using STM, they showed that the Ag nanostructures formed planar interfaces with Si(111) and that those multilayer structures were stable, with no coarsening at 300 K. In Fig. 1, we have replotted the cluster density when 0.2 *Å* Ag was deposited onto Xe as a function of the buffer thickness from Huang *et al.* For relatively low buffer thicknesses ($\theta \leqslant 50$ ML), there is a rapid decrease of density, an effect attributed to enhanced diffusion and aggregation boosted by the heat released from cluster–cluster coalescence.[11] Importantly, the cluster density follows a slower, well-defined power law decrease when the buffer thickness is large (~60–2000 ML).

Kashchiev[15] provided an analytic solution for the density of aggregating compact crystallites on a surface that is applicable to the low density Ag results, namely

$$\langle n\rangle = \kappa_0 C^{\gamma/(-3+\gamma)}(r_0^{\gamma} D_{r_0} t)^{-3/(3+\gamma)}, \tag{2}$$

where κ_0 is a parameter of order 1 that is dependent on γ, C is related to the average thickness h of the thin film, in the absence of surface wetting, through $C=3h/4\pi$, t is the total time available for diffusion, D_{r_0} is the diffusivity of a particle of radius r_0, and the power γ defines the dependence of the total diffusivity on particle radius r,

$$D(r) = D_{r_0}(r/r_0)^{-\gamma}. \tag{3}$$

In previous work,[11] we showed that the diffusivity of nanostructures in BLAG scales as the inverse of the contact area

with the buffer. For compact particles, the diffusivity scales as r^{-2} and $\gamma=2$.

The Kashchiev model excludes any dependence on temperature. In our experiments, however, temperature increases linearly with time during Xe desorption and nanostructure diffusion, and the model must be modified appropriately. For the purpose of our analysis, the temperature dependence on time can be written as $T(t)=\beta t$, where β is the warm-up rate. Thus, the time in Eq. (2) is intrinsically dependent on the thickness of the buffer layer θ, which desorbs according to

$$\theta(t) = \int_0^t A \exp\left[-\frac{\varepsilon_b}{k\beta t'}\right] dt', \tag{4}$$

where ε_b is the cohesive energy of Xe (0.167 eV) and A is the desorption prefactor for Xe [0.73×10^{12} s^{-1} (Ref. 16)]. In Ref.11, we used an approximate solution of Eq. (4), together with Eq. (2), to show that the power γ that describes the decay of cluster density increases linearly with the effective activation energy of cluster diffusion ε_d. A more accurate way to determine the particle diffusion parameters is to fit Eq. (2) numerically with the final densities of nanostructures grown on buffer layers of varying thickness, $\langle n(\theta)\rangle$, for a fixed warm-up rate. Since D_{r_0} is temperature dependent, as in Eq. (1), it is necessary to replace $D_{r_0}t$ in Eq. (2), which has the meaning of (diffusion length)^2 for a particle of radius r_0, with the integral of Eq. (1), $\int_0^t D_{00}\exp[-\varepsilon_d/(k\beta t')]dt'$. The numerical fit for θ in the range 60–2000 ML yields the effective activation energy and the prefactor for diffusion of Ag clusters on Xe, in the dilute limit. In particular, $\varepsilon_d=0.12\pm0.01$ eV and $D_{00}=5\times10^{-3}$ cm^2 s^{-1} for a single particle with $r_0=1$ nm. This pre-exponential is comparable in magnitude to the "usual value" of 10^{-3} cm^2 s^{-1} found in atomic self-diffusion on metal surfaces.[17] Thus, compact nanostructures of Ag on a highly incommensurate lattice of Xe have small barriers for diffusion and atomiclike pre-exponentials.

B. Compact particle aggregation: Dependence on the rate of temperature increase

Additional insights into nanostructure diffusion can be obtained by controlling the rate of warm-up, and hence the desorption rate of the rare gas solid, provided the particles are generally compact and large enough that the effect of the heat released from coalescence is negligible. These conditions are satisfied for nanostructures formed by the deposition of 1 Å of Au on Xe buffer layers of ~60 ML thickness. The density prior to warm-up is $\langle n\rangle=2\times10^{12}$ cm^{-2} and the mean radius of these particles is $\langle r\rangle=1$ nm. After warm-up at 1.5 K min^{-1} and soft landing on the a-C support, the density is $\langle n\rangle=5\times10^9$ cm^{-2} and the still-compact nanostructures have a mean radius $\langle r\rangle\sim5.5$ nm. Since the final density is determined by competition between cluster diffusion, $\exp(-\varepsilon_d/kT)$, and buffer desorption, $\exp(-\varepsilon_b/kT)$, it will also depend on the rate of warm-up. If, for instance, ε_d is larger than ε_b, the Xe desorption rate will increase faster than the particle diffusion rate as T increases and the buffer grows thinner. The desorption rate will then dominate, leading to less aggregation and a higher cluster density. The slower the warm-up rate, the more pronounced this effect will be since the buffer will be depleted at a lower temperature. Hence, a reduction in the warm-up rate β is accompanied by increased density if $\varepsilon_b<\varepsilon_d$. The opposite is expected when $\varepsilon_b>\varepsilon_d$, and no dependence on β is expected when the two energies are equal.

The argument presented above can be put on a quantitative basis if we assume that there are no significant changes in the Xe surface structure that accompany changes in β. The ratio between the final densities for two experiments, which differ only in β, follows from Eq. (2) when $D_{r_0}t$ is replaced by $\int_0^t D_{00}\exp[-\varepsilon_d/(k\beta t')]dt'$, namely

$$\frac{\langle n(\beta_1)\rangle}{\langle n(\beta_2)\rangle} = \left\{ \int_0^{t(\beta_1)} \exp[-\varepsilon_d/(k\beta_1 t')]dt' \Big/ \int_0^{t(\beta_2)} \exp[-\varepsilon_d/(k\beta_2 t')]dt' \right\}^{-3/(3+\gamma)}. \tag{5}$$

For a given buffer-layer thickness, $t(\beta)$ can be determined by numerically solving Eq. (4). Hence, the value of ε_d can be deduced from Eq. (5) if the dependence of density on warm-up rate is known.

Figure 2 summarizes the dependence of cluster density on warm-up rate for β ranging from 0.05 to 2.75 K min^{-1} (the time between the desorption of the first and the 60th monolayer ranged from 180 to 4 minutes, respectively). The density was $\langle n\rangle=3\times10^{10}$ cm^{-2} for $\beta=0.05$ K min^{-1}, but it was much lower, 5×10^9 cm^{-2}, for $\beta=1.5$ K min^{-1}. Thus $\varepsilon_b<\varepsilon_d$, and desorption of Xe is the dominant process. The dashed lines show how $\langle n\rangle$ would vary with β for several different values of ε_d, normalized to an initial point at 1 K min^{-1}. The best fit to the experimental data is the solid line, corresponding to $\varepsilon_d=0.29\pm0.05$ eV. The spread is due to the relatively small variation of $\langle n\rangle$ over the experimentally-accessible range of β. From Eqs. (1) and (2) using $\varepsilon_d=0.29$ eV, we find a pre-exponential factor of $D_{00}=9\times10^9$ cm^2 s^{-1} for $r_0=1$ nm. Both ε_d and D_{00} are significantly higher than the values found for small Ag clusters, as discussed below.

C. Aggregation in the incomplete coalescence regime: Experiment and Monte Carlo simulations

The transition from compact particles to ramified structures occurs when there is insufficient time to allow a growing particle to assume a compact structure before a new particle arrives. The transition then depends on the energy barriers that control the approach to an equilibrium shape and the size of the particles involved. Our results show the evolution of the diffusing species, both in the compact regime and in the incomplete coalescence regime.

To gain insight into the diffusive properties of nanostructures in the incomplete coalescence regime, we deposited 5 Å films of Cu, Au, Pd, Co, and Ni on Xe buffer layers with thickness ranging from 4 to 120 ML. After deposition, the samples were warmed at $\beta=1.66$ K min^{-1}. Analysis of results for $\theta>10$ ML indicates that the fraction of the surface covered by the islands was substantial, namely 0.12 for Au,

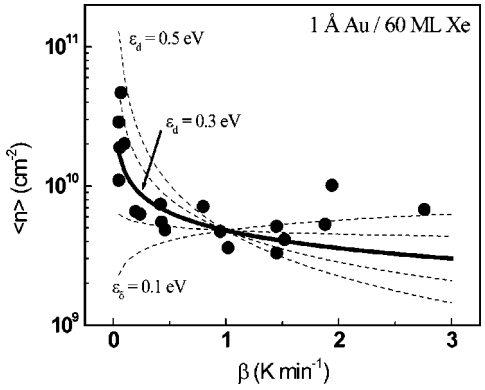

FIG. 2. The data points show how the cluster density depends on the warm-up rate. The time between the desorption of the first and the 60th monolayer ranged from 180 min for $\beta = 0.05$ K min^{-1} to 4 min for $\beta = 2.75$ K min^{-1}. The drop in $\langle n \rangle$ with increasing β indicates that $\varepsilon_b < \varepsilon_d$ and Xe desorption is the dominant process in dictating $\langle n \rangle$. The dashed lines are calculated from Eq. (5), normalized at $\beta = 1$ K min^{-1}. The solid line is the best fit, giving $\varepsilon_d = 0.29 \pm 0.05$.

0.16 for Cu, 0.26 for Pd, 0.13 for Co, and 0.22 for Ni. The upper portion of Fig. 3 shows representative TEM micrographs after growth for buffer-layer thicknesses of 30–32 ML, as imaged on the a-C substrate. For Au the branches are well developed but not as extended as those for Pd, and the morphologies for Cu, Co, and Ni, are intermediate between these extremes. Thus, aggregation is greatest for Pd and least for Au, reflecting the different rates of island diffusion. Typical branch widths range from ~8 for Ni to ~11 nm for Cu, reflecting the different rates of coalescence characteristic for these materials. Silver was also studied, but the very low barrier for Ag atom self-diffusion allowed the islands to undergo significant shape changes at room temperature. The result was fragmentation of the branches and balling-up of the fragments.

The bottom of Fig. 3 shows the cluster density $\langle n \rangle$ for different Xe buffer layers for Au, Cu, Co, Ni, and Pd with straight lines that represent fits to the power-law decay. The slopes then emphasize the differences in the decay rates for the different metals. As observed previously for Au growth on Xe, Kr, and Ar,[10,11] we see a power law dependence $\langle n \rangle \propto \theta^y$ where $y = -2.41 \pm 0.09$ (Au), -2.34 ± 0.14 (Cu), -3.12 ± 0.12 (Pd), -2.53 ± 0.14 (Co), and -3.52 ± 0.20 (Ni). These exponents reflect the different rates of increase of diffusivity with temperature and the different surface coverages characteristic for each metal, as discussed in the following.

The fact that the incomplete coalescence regime is characterized by a constant average island height[11] suggests that the theoretical formalism developed for two-dimensional diffusion-limited cluster–cluster aggregation (DLCCA) is suitable for its analysis. For instance, according to the analysis by Kolb,[18] the island density is expected to vary with time as

$$\langle n \rangle \propto (D_{S_0} t)^z, \tag{6}$$

where $z = -1/(1+\alpha)$, and D_{S_0} is the diffusivity of a particle of area S_0, assuming diffusivity of the form $D(S) = D_{S_0}(S/S_0)^{-\alpha}$ where S is the area of the two-dimensional island. Note that the proportionality (6) is also valid for compact particles, as it follows from Eq. (2) with $\gamma = 2\alpha$.

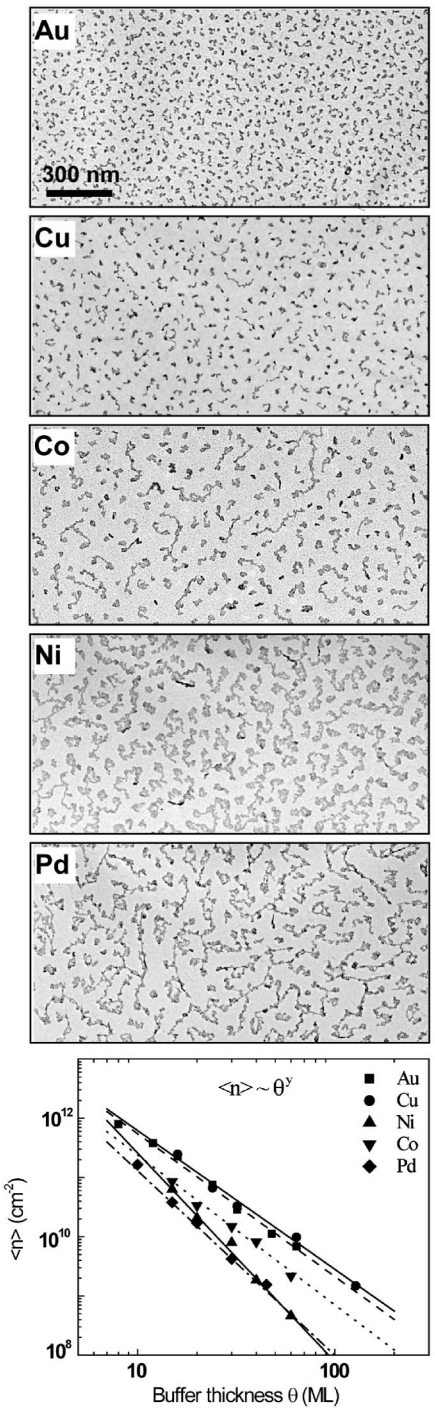

FIG. 3. Top: TEM micrographs of metallic nanostructures produced from the deposition of 5 Å Au, Cu, Co, Ni, and Pd on 30–32 ML Xe. These are ramified islands because the impingement rate is too high and the atom diffusion on the cluster is too low to produce compact structures. Typical branches have widths and heights that are ~10 nm. Bottom: Island densities as a function of buffer thickness. The effective activation energies are calculated from the slopes, and the prefactors are deduced with the help of Monte Carlo simulations.

Kolb's analysis was restricted to the dilute limit. Lach-hab *et al.* studied the effect of finite concentration on three-dimensional colloid aggregation, assuming that the diffusivity varied with size S as $D(S) \propto S^{-1/d}$, where the fractal dimension d increased with size.[19] They found that the power law exponent of growth of the weighted average cluster size increased significantly with the fraction of space occupied.

To determine the effects of surface coverage for our experiments, we therefore carried out Monte Carlo simulations of DLCCA in two dimensions with surface coverages, ρ, between 0.01 and 0.35. The simulation space was a square lattice with periodic boundary conditions as depicted in Fig. 4(a). At the beginning of each simulation, a predetermined number of cells were randomly occupied, with lone occupied cells or nearest-neighbor cells counting as single clusters. Subsequently, clusters were chosen at random to translate, as a whole, a unit step in a random direction [the arrow in Fig. 4(a)]. The probability for a chosen cluster to move was $1/N_c$, where N_c is the number of the occupied cells forming the cluster. In this way, a cluster occupying a single cell had a diffusion length l (the length of a single cell) each time it is chosen to move. Larger clusters occupying N_c cells had the same diffusion length but only after they had been chosen N_c times on the average. This makes it possible to follow particle kinetics in which the diffusivity is inversely proportional to the area it covers. Each time a cluster was chosen to move, the system time was increased by $1/N$, where N was the total number of clusters at that time, regardless of whether the cluster was moved or not. This was done to ensure that every cluster was chosen on the average once per unit simulation time $\Delta t'$. The diffusivity of the clusters was therefore determined by $D(N_c) = l^2/(4N_c\Delta t')$. When a cluster arrived at a cell that was adjacent to another cluster, the two were conjoined. The simulation was continued for a predetermined number of steps, or until only a single cluster remained.

Representative images of a portion of the simulation space at $\rho = 0.1$ are shown in Fig. 4(b). Comparison with the TEM images in Fig. 3 shows a good degree of morphological similarity.[20] The advance of aggregation at different moments in simulation time t' is evident, and the number of clusters asymptotically approached a power-law dependence on time $N \propto t'^z$. Figure 4(c) summarizes the results of a large number of simulations with coverages ρ of 0.01–0.35 where the power z is plotted as a function of the fractional surface coverage. In the dilute limit, $z = -0.5$, in agreement with the theoretical estimate[18] for $\alpha = 1$. Significantly, z depends linearly on ρ for $\rho \leqslant 0.35$, namely $z = -0.5 - (2.46 \pm 0.03)\rho$. This increase in the magnitude of z supports our earlier qualitative reasoning that the decay would be faster for ramified islands than for compact clusters because the former would have to travel shorter distances in order to aggregate.[11] Here, the numerical estimates of z and the prefactor made it possible to analyze quantitatively the density decay curves obtained from the BLAG experiments.

The ratio between the final density in two experiments, where only the buffer-layer thickness θ is different, follows from Eq. (6) where $\int_0^t D_{00} \exp[-\varepsilon_d/(k\beta t')]dt'$ is substituted for $D_{S_0} t$, namely

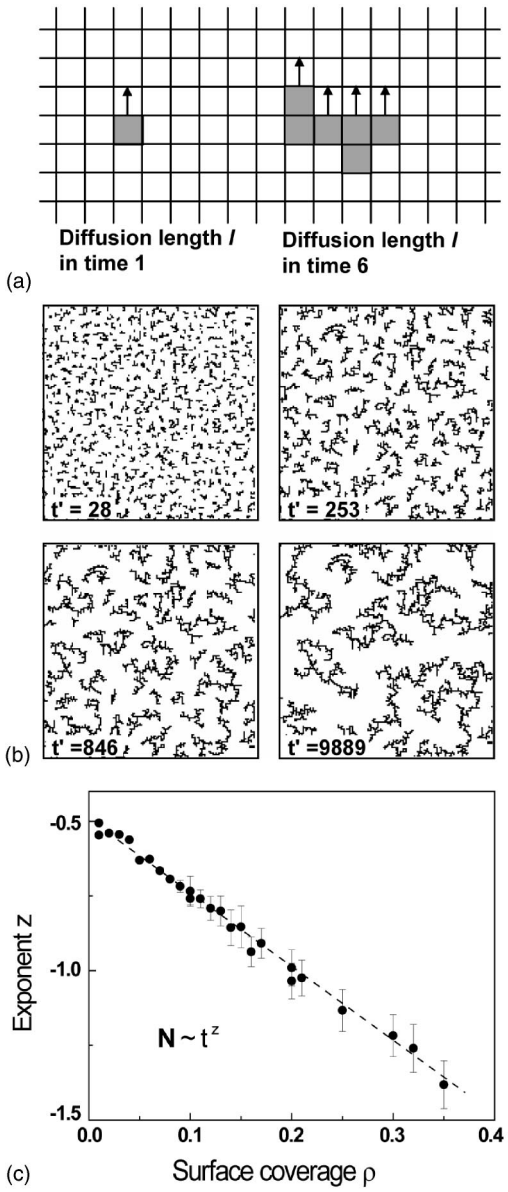

FIG. 4. (a) Diffusion in the Monte Carlo simulation of diffusion-limited cluster–cluster aggregation. Each cluster diffuses on the square lattice with a diffusivity that is inversely proportional to the area covered by the cluster. Both clusters are depicted as moving one unit cell in a time interval corresponding to their size. (b) Snapshots of a portion of simulation space at different times at 0.1 coverage, showing the advance of aggregation with time. (c) Exponent of decay in the power-law island number decay $N \propto t'^z$, as a function of the fraction of space occupied. The magnitude of z increases linearly from the theoretically predicted value of 0.5 in the dilute limit.

$$\frac{\langle n(\theta_1)\rangle}{\langle n(\theta_2)\rangle} = \left\{ \int_0^{t(\theta_1)} \exp[-\varepsilon_d/(k\beta t')]dt' \Big/ \int_0^{t(\theta_2)} \exp[-\varepsilon_d/(k\beta t')]dt' \right\}^z, \tag{7}$$

where $z = z(\rho)$ is the coverage-dependent rate of island den-

TABLE I. Summary of the determined diffusion parameters for compact and ramified nanostructures on solid Xe. $\langle S \rangle$ is the average projected area of a particle in the experiment and ε_d is the effective activation is size-independent (Ref. 11). D_{00} is the prefactor for a model particle of 100 nm^2 projected area. Values for the diffusivity of such a model particle are given in the text for a specific temperature, corresponding to the desorption of part of the buffer layer. These energies and prefactors are plotted in Fig. 5 and discussed in the text in terms of the compensation effect.

Material	Morphology	Experimental $\langle S \rangle (nm^2)$	ε_d(eV)	$D_{00}(cm^2\ s^{-1})$
Ag	Compact clusters	4	0.12 ± 0.01	2×10^{-4}
Au	⋯	100	0.29 ± 0.05	3×10^{8}
Au	Ramified islands	$10^3 - 10^5$	0.53 ± 0.02	3×10^{21}
Cu	⋯	⋯	0.46 ± 0.03	3×10^{16}
Pd	⋯	⋯	0.48 ± 0.02	1×10^{19}
Co	⋯	⋯	0.54 ± 0.03	5×10^{22}
Ni	⋯	⋯	0.60 ± 0.04	3×10^{26}

sity decay. Therefore, ε_d can be found using Eq. (7) once the dependence $\langle n(\theta) \rangle$ is known, assuming that ρ deduced from the TEM images is not significantly different from that during the aggregation events. Using the results summarized in Fig. 3, we find that $\varepsilon_d = 0.46 \pm 0.03$ (Cu), 0.48 ± 0.02 (Pd), 0.53 ± 0.02 (Au), 0.54 ± 0.03 (Co), and 0.60 ± 0.04 eV (Ni).

The total diffusion coefficient for ramified islands can be deduced by comparing the results from experiment and simulation. In the simulation, a particle with a size of a single cell in the 2D lattice has a fixed diffusivity given by $D = l^2/(4\Delta t')$, where l is the unit cell size and $\Delta t'$ is a unit simulation time, Fig. 4(a). To deduce the experimental D, it is necessary to find the corresponding real world substitutes for the parameters l and $\Delta t'$. Since the typical width of an island branch in the simulation was l, a suitable real value for l is 10 nm, the characteristic branch width of our ramified islands. Assigning a value to the lattice cell size yields a real number for the density of islands at a given time t'. Therefore, the dependence of simulation time t' on the real time t can be found numerically by finding the simulation time t' that yields the same cluster density as the experiment does at time t. $\Delta t'$ can then be substituted with $\Delta t' = [dt'(t)/dt]\Delta t$, thus yielding the dependence $D(t)$, which is exponential since T increases linearly with t in the experiments.

Table I summarizes the measured values of the effective activation energies for diffusion, ε_d, which is independent of particle size.[11] Also shown is the diffusion prefactor D_{00} [Eq. (1)]. Since D_{00} depends on size, the numbers are given for a model particle of projected area of 100 nm^2. This model particle is then much smaller than the experimental areas of the ramified islands measured after complete desorption. The prefactors for the ramified islands ranged from 3×10^{16} $cm^2\ s^{-1}$ for Cu to 3×10^{26} $cm^2\ s^{-1}$ for Ni. According to these numbers, a Au particle of 100 nm^2 projected area would have a total diffusivity of 1.6×10^{-14} $cm^2\ s^{-1}$ after the desorption of the first 10 ML of Xe, as the sample is warmed at 1.66 K min^{-1}, using $D_{00} \exp(-\varepsilon_d/kT)$ with $T = 75.9$ K. This diffusivity would increase several orders of magnitude to 3.7×10^{-12} $cm^2\ s^{-1}$ after 60 ML desorption (where $T = 81.2$ K). A Pd island of the same area would have a diffusivity that would increase from 2.1×10^{-13} to 2.8×10^{-11} $cm^2\ s^{-1}$.

The value of $\varepsilon_d = 0.53$ eV for ramified Au islands cited above is larger than the 0.29 eV measured for compact Au clusters in the preceding section. This conflicts with our model which suggests constant ε_d [Eq. (1)], on the basis of the observation of a constant slope in the dependence $\langle n(\theta) \rangle$ as in Fig. 3.[11] There are two possible explanations. The first is that ε_d does increase slightly with particle/buffer contact area (the contact area varies by as much as three orders of magnitude when compact islands are compared to ramified islands), but the changes in the slope of $\langle n(\theta) \rangle$ are too small to be distinguished. If this is the case, the measured values for ε_d should be regarded as average values. Alternatively, there might be a dependence of ε_d on the particle morphology such that it is higher for ramified islands than for compact clusters.[21] In either case, the total diffusion coefficient (Table I) for a Au particle of given projected area is higher when deduced from the aggregation of small compact clusters rather than from large ramified islands, and this should be expected to hold for all materials.

It is intriguing to compare the values for the activation energy for diffusion found so far with the binding energies of rare gas atoms on metal surfaces. Vidali *et al.*[22] report 0.214 eV for Xe on Au(111), 0.183 eV for Xe on Cu(111), and 0.356 eV for Xe on Pd(111), where the on-top adsorption sites are preferred.[23] The ratio of the values for Xe/Au(111) and Xe/Cu(111), 1.17, is very close to the ratio $\varepsilon_d^{Au}/\varepsilon_d^{Cu}$ for ramified islands on solid Xe, namely 1.16. On the other hand, ε_d found for Pd islands is lower than what would be expected from an equivalent scaling of the Xe/Pd(111) data. This suggests that the details of the lattice mismatch at the island/buffer interface may play a role in determining ε_d, supplementing the single atom electronic interactions. In any case, it is fascinating that the diffusion barrier for such large ramified features is such a small number, amounting to only ~2.5 times the binding energy of a single Xe atom to Au and Cu and 1.4 times that to Pd.

D. Compensation effect

The pre-exponents for diffusion D_{00} in Table I are extraordinarily large.[24] While an Arrhenius behavior, $D_{00} \exp(-\varepsilon_d/kT)$, holds, cluster diffusion is very different

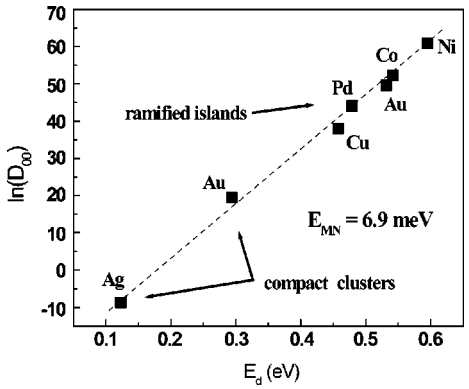

FIG. 5. The calculated prefactors D_{00} extrapolated for a model particle of 100 nm^2 projected area of Ag and Au (compact) and Cu, Pd, Au, Co, and Ni (ramified) as a function of the effective activation energy for diffusion for each material. The dependence is exponential, indicating that nanoparticle diffusion follows a Meyer–Neldel rule with a characteristic energy of 6.9 meV. The latter is comparable to the energy of the phonon excitations in solid Xe ($E_{\mathrm{Debye}}=5.5$ meV).

from atom diffusion in a corrugated potential, where ε_d is a well-defined potential barrier and D_{00} is proportional to the vibrational frequency. In fact, as the molecular dynamics simulation by Deltour *et al.* demonstrated,[25] the cluster diffusion trajectory on an incommensurate surface does not reflect at all the potential corrugation. In addition, the many-body character of multiatom cluster motion is expected to contribute to the entropy of the process, thus increasing the prefactor.

Insight into the microscopic origin of the large prefactors in nanostructure diffusion comes from Fig. 5 where we plot $\ln(D_{00})$ vs ε_d for Ag, Cu, Pd, Au, Co, and Ni for model islands of 100 nm^2 projected area. The dashed line, which is a fit to the data, shows a remarkable exponential dependence over a range of 30 orders of magnitude. Such behavior, in which the prefactor in an Arrhenius relation $A\exp(-E/kT)$ varies as

$$A(E) \propto \exp(E/E_{\mathrm{MN}}) \tag{8}$$

is known as the compensation effect or the Meyer–Neldel rule (MNR) and it is characterized by the Meyer–Neldel energy (E_{MN}). Yelon and Movaghar[26,27] have argued that the compensation effect is to be expected whenever the activation energy for a process is large compared to the energy of the typical fluctuations in the system. In their work, they demonstrated that the number of ways these fluctuations can assemble to trigger such a process increases exponentially with the activation energy, in agreement with the Meyer–Neldel rule. For nanostructures diffusing on solid Xe, the above condition is clearly satisfied since the Debye energy of solid Xe is only 5.5 meV and the deduced effective activation energies for nanoparticle diffusion are two orders of magnitude higher. Hence, we conclude that the compensation effect in nanostructure diffusion on Xe is a manifestation of the many-body nature of diffusion excitation by phonons.

In more recent works, Yelon *et al.*[27] and Boisvert *et al.*[28] revisited a number of data from experiments and simulation for which the Meyer–Neldel rule is observed. They found that E_{MN} is typically a few times the energy of the fluctuations in the system. The characteristic Meyer–Neldel energy follows from the slope of the dashed line in Fig. 5, namely $E_{\mathrm{MN}}=6.9$ meV. This energy is in fair agreement with the energy of the longitudinal-phonon maximum in the density of phonon states of solid Xe, namely 5.1 meV.[29]

The total diffusivity of particles of the different metals studied here varies over an order of magnitude for a given size. It is a remarkable consequence of the compensation effect, however, that particles of different metals exhibit very similar diffusivities despite the significant differences in ε_d. It will be of interest to determine at the atomic level the origins for the observed diffusive properties of these nanoscopic and mesoscopic particles on rare-gas solid surfaces.

IV. SUMMARY

We have determined for the first time values for the diffusion parameters of clusters and extended nanostructures on solid Xe where the diffusion is thermally activated. The values, obtained from a series of BLAG experimental results, were interpreted with the help of existing theories of cluster–cluster aggregation, and are summarized in Table I. For Ag clusters a few nm across, we find $\varepsilon_d=0.12$ eV and a pre-exponential factor that is comparable to the values observed in atomic diffusion on surfaces.

To interpret the data for ramified island aggregation, we carried out Monte Carlo simulation of diffusion-limited cluster–cluster aggregation in two dimensions and studied the changes in the parameters of growth as a function of the fraction of space occupied. These results showed that the magnitude of the exponent of growth increased linearly with surface coverage from its accepted theoretical value in the dilute limit.

For extended ramified islands covering 10^3-10^5 nm^2, we deduced activation energies in the range of 0.46–0.60 eV and gigantic prefactors (Table I). The latter are attributed to the many-body character of cluster/nanostructure diffusion. These diffusion parameters follow a Meyer–Neldel-type compensation rule with a characteristic Meyer–Neldel energy of 6.9 meV, comparable to the energy of the elementary phonon excitations in solid Xe. In view of previous observations of large pre-exponential factors,[24] we expect this to be a general characteristic of the activated processes at the mesoscale.

ACKNOWLEDGMENTS

This work was supported in part by the U.S. Army Research Office and in part by the U.S. Department of Energy, Division of Materials Sciences under Grant Nos. DEFG02-01ER45944 and DEFG02-91ER45439 through the Frederick Seitz Materials Research Laboratory. We thank C.M. Aldao for many useful discussions. A.S.B. acknowledges support from the Fulbright Commission and CIES; P.S.W. was supported under the NSF research experience for undergraduates program.

*Permanent address: Department of Physics, COMSATS Institute of Information Technology, Sector H-8/1, Islamabad, Pakistan.

[1] A. G. Naumovetz and Z. Y. Zhang, Surf. Sci. **500**, 414 (2002).

[2] P. Jensen, Rev. Mod. Phys. **71**, 1695 (1999).

[3] L. Huang, S. J. Chey, and J. H. Weaver, Phys. Rev. Lett. **80**, 4095 (1998).

[4] G. D. Waddill, I. M. Vitomirov, C. M. Aldao, S. G. Anderson, C. Capasso, J. H. Weaver, and Z. Liliental-Weber, Phys. Rev. B **41**, 5293 (1990).

[5] G. D. Waddill, I. M. Vitomirov, C. M. Aldao, and J. H. Weaver, Phys. Rev. Lett. **62**, 1568 (1989).

[6] See Ref. 3 for growth on Si. See Ref. 5 for growth on GaAs. For growth on high-temperature superconductors, see T. R. Ohno, Y.-N. Yang, G. H. Kroll, K. Krause, L. D. Schmidt, J. H. Weaver, Y. Kimachi, Y. Hidaka, S. H. Pan, and A. L. de Lozanne, Phys. Rev. B **44**, 2430 (1991); T. R. Ohno, Y.-N. Yang, J. H. Weaver, Y. Kimachi, and Y. Hidaka, Appl. Phys. Lett. **57**, 718 (1990).

[7] J. H. Weaver and G. D. Waddill, Science **251**, 1444 (1991).

[8] K. Yoo, A. P. Li, Z. Y. Zhang, H. H. Weitering, F. Flack, M. G. Lagally, and J. F. Wendelken, Surf. Sci. **546**, L803 (2003).

[9] K. Yoo, Z. Y. Zhang, and J. F. Wendelken, Jpn. J. Appl. Phys., Part 2 **42**, L1232 (2003).

[10] C. L. Haley and J. H. Weaver, Surf. Sci. **518**, 243 (2002).

[11] V. N. Antonov, J. S. Palmer, A. S. Bhatti, and J. H. Weaver, Phys. Rev. B **68**, 205418 (2003).

[12] V. N. Antonov and J. H. Weaver, Surf. Sci. **526**, 97 (2003).

[13] W. Meyer and H. Neldel, Z. Tech. Phys. (Leipzig) **12**, 588 (1937).

[14] A. Zangwill, *Physics at Surfaces* (Cambridge University Press, Cambridge, England, 1988).

[15] D. Kashchiev, Surf. Sci. **55**, 477 (1976).

[16] J. A. Venables, *Introduction to Surface and Thin Film Processes* (Cambridge University Press, Cambridge, England, 2000).

[17] G. L. Kellogg, Surf. Sci. Rep. **21**, 1 (1994).

[18] M. Kolb, Phys. Rev. Lett. **53**, 1653 (1984).

[19] M. Lach-hab, A. E. Gonzalez, and E. Blaisten-Barojas, Phys. Rev. E **54**, 5456 (1996).

[20] The somewhat higher linearity in the TEM images can be attributed to some post-deposition compactization of the smallest features of the fractal islands at room temperature. This would decrease their short-range fractal dimension. H. F. van Garderen, W. H. Dokter, T. P. M. Beelen, R. A. van Santen, E. Pantos, M. A. J. Michels, and P. A. J. Hilbers, J. Chem. Phys. **102**, 480 (1995).

[21] Lower diffusivity of branched clusters compared to compact clusters of the same size has been reported in a recent study of diffusion of Ag micro-aggregates on a silicone oil surface. G.-X. Ye, T. Michely, V. Weidenhof, I. Friedrich, and M. Wuttig, Phys. Rev. Lett. **81**, 622 (1998).

[22] G. Vidali, G. Ihm, H. Y. Kim, and M. W. Cole, Surf. Sci. Rep. **12**, 133 (1991).

[23] J. L. F. Da Silva, C. Stampfl, and M. Scheffler, Phys. Rev. Lett. **90**, 066104 (2003).

[24] Such large values were also measured in the only previous work (to our knowledge) that studied rigid diffusion of nanostructures on a solid surface. In that work, the nanostructures were mass-selected 2300-atom Sb clusters on graphite, and the authors deduced that $\varepsilon_d = 0.7$ eV and $D_{00} = 10^4$ cm^2 s^{-1}. They attributed this large prefactor to the collective character of mesoscopic particle motion, i.e., motion without rearrangement of the constituent atoms. L. Bardotti, P. Jensen, A. Horeau, M. Treilleux, and B. Cabaud, Phys. Rev. Lett. **74**, 4694 (1995).

[25] P. Deltour, J. L. Barrat, and P. Jensen, Phys. Rev. Lett. **78**, 4597 (1997).

[26] A. Yelon and B. Movaghar, Phys. Rev. Lett. **65**, 618 (1990).

[27] A. Yelon, B. Movaghar, and H. M. Branz, Phys. Rev. B **46**, 12 244 (1992).

[28] G. Boisvert, L. J. Lewis, and A. Yelon, Phys. Rev. Lett. **75**, 469 (1995).

[29] *Rare Gas Solids*, edited by M. L. Klein and J. A. Venables (Academic, New York, 1977), Vol. II.